High rates of sea-level rise during the last interglacial period

E. J. ROHLING[1]*, K. GRANT[1], CH. HEMLEBEN[2]*, M. SIDDALL[3], B. A. A. HOOGAKKER[4], M. BOLSHAW[1] AND M. KUCERA[2]

[1]National Oceanography Centre, European Way, Southampton SO45 5UH, UK
[2]Institute of Geosciences, University of Tübingen, Sigwartstrasse 10, 72076 Tübingen, Germany
[3]Lamont-Doherty Earth Observatory, 61 Route 9W - PO Box 1000, Palisades, New York 10964-8000, USA
[4]Department of Earth Sciences, University of Cambridge, Downing Street, Cambridge CB2 3EQ, UK
*e-mail: E.Rohling@noc.soton.ac.uk; christoph.hemleben@uni-tuebingen.de

Published online: 16 December 2007; doi:10.1038/ngeo.2007.28

The last interglacial period, Marine Isotope Stage (MIS) 5e, was characterized by global mean surface temperatures that were at least 2 °C warmer than present[1]. Mean sea level stood 4–6 m higher than modern sea level[2–13], with an important contribution from a reduction of the Greenland ice sheet[1,14]. Although some fossil reef data indicate sea-level fluctuations of up to 10 m around the mean[3–9,11], so far it has not been possible to constrain the duration and rates of change of these shorter-term variations. Here, we use a combination of a continuous high-resolution sea-level record, based on the stable oxygen isotopes of planktonic foraminifera from the central Red Sea[15–18], and age constraints from coral data to estimate rates of sea-level change during MIS-5e. We find average rates of sea-level rise of 1.6 m per century. As global mean temperatures during MIS-5e were comparable to projections for future climate change under the influence of anthropogenic greenhouse-gas emissions[19,20], these observed rates of sea-level change inform the ongoing debate about high versus low rates of sea-level rise in the coming century[21,22].

It is well established that past rates of sea-level rise due to ice-volume reduction have reached up to 5 m per century[23–25]. However, such values relate to deglaciations, dominated by disintegration of the now-absent Laurentide ice sheet, which questions their suitability for projections of future sea-level change within a well-developed interglacial period. So far, no detailed information exists about the rates of sea-level change associated with fluctuations within interglacial periods in general, and above 0 m in particular. This focuses attention on MIS-5e, the most recent (best dated) interglacial period during which sea level stood several metres above 0 m between roughly 124 and 119 kyr (thousand years ago) (see the Supplementary Information).

MIS-5e warmth was caused by orbital forcing of insolation, rather than the predicted greenhouse forcing of the near future, so that MIS-5e ice-volume responses may have differed in detail from future responses. However, we do not consider the MIS-5e warming as a straight analogy to the future, but instead aim to provide an observational context that quantifies the potential range of sea-level change rates above 0 m, to inform the debate about ice-volume reduction/sea-level rise in the next century that currently relies entirely on theoretical projections[21,22].

By dating fossil corals, previous studies have established that MIS-5e sea level reached an average highstand around +4 (±2) m, with individual maxima up to +7 or +9 m (refs 2–13) (see the Supplementary Information). Up to 5 m of this signal derived from reduction of the Greenland ice sheet[14]. There may also have been contributions from (West) Antarctica, which is responsive to climate change[26], although models suggest a slow and gradual response[22].

Although dated corals yield impressive insight into sea-level position and absolute age, they lack the tightly constrained relative-age framework needed to calculate rates of change. We overcome that problem by combining coral data with a new, continuous, highly resolved sea-level reconstruction through MIS-5e from the recent calibration method for central Red Sea stable oxygen isotope (δ^{18}O) records[15–18], which offers tight stratigraphic control of relative ages.

Figure 1a shows new high-resolution δ^{18}O data from the MIS-6–5e deglaciation[15] through MIS-5e in central Red Sea sediment core GeoTü-KL11, superimposed on the previously published low-resolution record of KL11 for the entire MIS-6–4 interval[17,27] (see the Methods section). Also shown is a new 0.5–2-cm-resolution δ^{18}O record through MIS-5 from nearby core GeoTü-KL09, superimposed on a whole-core 10-cm-resolution record for that core (see the Methods section). Throughout this letter, records from cores KL11 and KL09 are correlated in the depth domain on the basis of simple linear matching between MIS-4 and the onset of MIS-5e, without any subjective 'fine-tuning' (Fig. 1a–d).

Figure 1b,d shows the δ^{18}O data converted into sea-level estimates, using the calibration developed for KL11 ($1\sigma = 6$ m) (see the Methods section)[15,17,18]. A first important observation is that sea level according to KL09 reached a shallowest value of about −17 m during MIS-5c, compared with about −40 m (or −30 m on the basis of low-resolution results of KL11) during MIS-5a (Fig. 1b). The MIS-5c value agrees with Barbados coral terraces, which suggest that sea level reached up to −16 m during both periods[28], but the MIS-5a value seems low relative to Barbados. We have yet to fully resolve MIS-5a, and consider our MIS-5c estimate more definitive than the MIS-5a value.

Figure 2 concentrates on MIS-5e in both KL11 and KL09, compared with a detailed series of coral-based sea-level estimates from Barbados[4]. The Red Sea results are shown versus depth in each core, and the KL11 series was calibrated to age by linearly matching

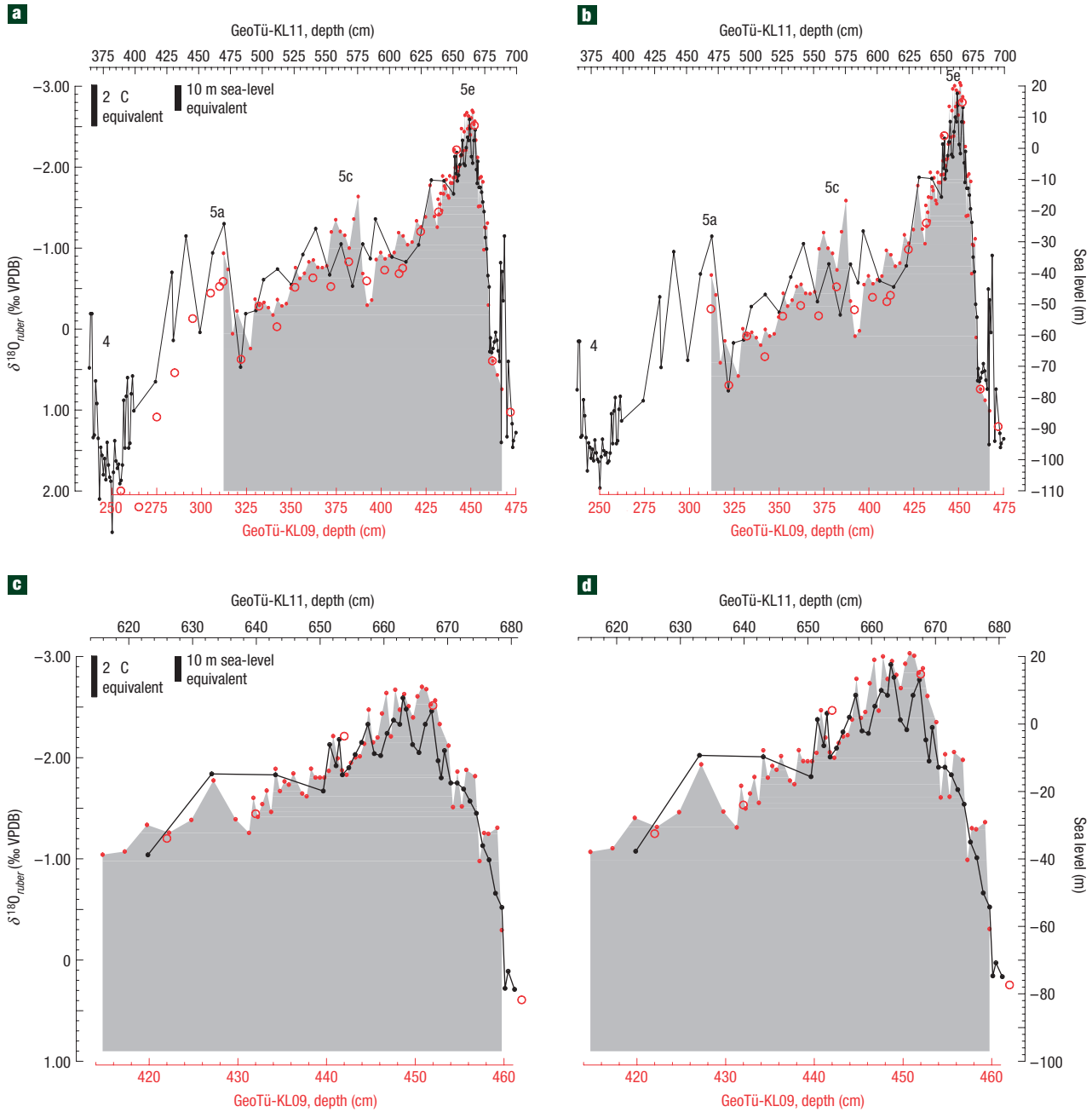

Figure 1 Stable isotope and derived sea-level records for central Red Sea cores KL11 and KL09. a, $\delta^{18}O_{ruber}$ throughout MIS-5e–4 for KL11 (black filled circles, line), alongside high-resolution data (red filled circles, grey shading) and a low-resolution series (red open circles) for KL09 (see the Methods section; VPDB: Vienna PeeDee Belemnite). Black bars indicate amplitudes of $\delta^{18}O$ change equivalent to about 2 °C temperature change and 10 m of sea-level change. The numbers identify Marine Isotope Stages. **b**, As **a**, but for sea level as derived from $\delta^{18}O_{ruber}$ (refs 17,18). **c**, As **a**, but magnified for a detailed comparison of trends within MIS-5e. **d**, As **c**, but for derived sea level.

the 'inverted U' shape of its long-term average sea-level trend to that in the dated corals[4] (Fig. 2a). Within MIS-5e, we maintain our straightforward linear KL11–KL09 correlation (Fig. 1a), so that the correlation of KL11 to the dated corals (Fig. 2a) implicitly yields an approximate age model for KL09 (Fig. 2b).

A 3,000 yr gaussian filter through KL11 reveals a long-term mean MIS-5e highstand up to +6 m, in agreement with the coral data (Fig. 2a). The same filter through KL09 reveals a comparable pattern (Fig. 2b) (see the Methods section). Shorter-term fluctuations are evaluated using a 750 yr filter through both records (Fig. 2c,d). Here, the two Red Sea records differ: the distinct fluctuations seen in KL11 are poorly/not represented in KL09 (Fig. 2c,d). Although this apparent discrepancy probably reflects different impacts of bioturbation in the two cores (see the Methods section), it does highlight a need for qualification of our results in terms of 'robustness'. Accordingly, we first identify a detailed record of sea-level oscillations within MIS-5e on the basis of KL11, then investigate to what extent this record is supported by

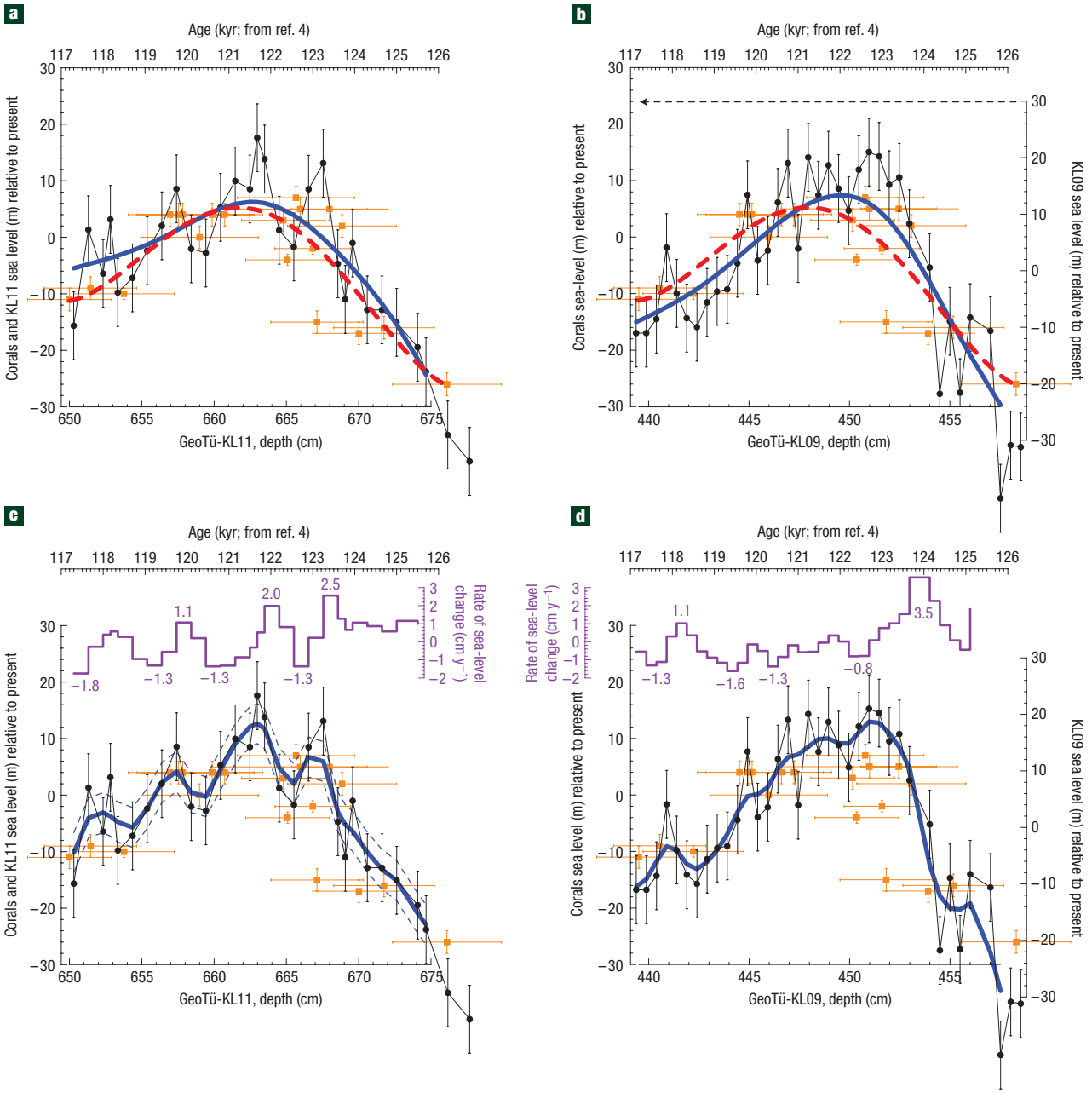

Figure 2 MIS-5e high-resolution Red Sea sea-level reconstruction for KL11 and KL09 versus coral data. KL11 and KL09: black lines/filled circles, $1\sigma = 6$ m error bars[17,18]; coral data: orange squares, with age/altitude error bars[4]. **a**, Long-term average trends: 3,000 year gaussian filter through KL11 (thick blue line); long-term trend in coral data (dashed red line). **b**, As **a**, for KL09. **c**, Short-term sea-level trends, from a 750 year gaussian filter through KL11 (thick blue line). Dashed blue lines show statistical 1 standard error for this record. The first time derivative of the thick blue record yields rates of change (purple step plot, with maximum rates of rise (positive) and lowering (negative)). **d**, As **c**, for KL09.

previous work, and finally identify which of the inferred features are most robust in that they are also obvious in KL09.

The $1\sigma = 6$ m uncertainty in the Red Sea sea-level method includes a ± 1 °C uncertainty in sea surface temperature (SST) and a generous uncertainty for net evaporation[17,18]. To minimize the influence of any bias in individual points, we infer MIS-5e sea-level fluctuations after smoothing the data with a moving 750 yr gaussian filter (Fig. 2c). With $1\sigma = 6$ m for individual points, the standard error of the filtered mean sea-level record in KL11 is determined in a statistical sense for this particular data set (Monte Carlo method) at 1 standard error = 3.5 m (Fig. 2c). This yields the first sea-level record with the essential attributes (high temporal resolution and stratigraphic continuity) for quantification of rates of change associated with millennial-scale oscillations within MIS-5e. First, however, we consider whether there is support from other, independent sea-level indicators for the inferred oscillations (Fig. 2c). Ages reported for the Red Sea record are subject to the about ± 1 kyr uncertainty margin of the coral datings that underlie our age model[4] (Fig. 2a). However, the tightly constrained stratigraphic order of our records stipulates that such

age uncertainties will be systematically distributed along the record, so that age uncertainties are much smaller than ±1 kyr where relative sample ages (hence, durations) are concerned.

Although some studies of MIS-5e corals favour a single highstand rather than a compound structure[2,3,13], there is a hiatus in the Western Australian record[3] that may agree with suggestions of intra-MIS-5e sea-level instability around 122 ± 1 kyr in fossil reef records from Barbados[4], the Bahamas[3,8,9] and the Red Sea[5–7,11,12] (see Supplementary Information, Table S1). KL11 suggests two main highstands around 123 and 121.5 kyr, separated by a relative lowstand around 122.5 kyr (Fig. 2c). A third minor highstand is suggested around 119.5 kyr, after a relative lowstand centred on 120.5 kyr. The amplitude of the latter fluctuation, as well as that of the sea-level drop following the 119.5 kyr high, is well supported by the coral data[4] (Fig. 2c). The same holds for the early MIS-5e rise into the first highstand of 123 kyr (Fig. 2c), and it was previously found that detailed sea-level fluctuations inferred from the Red Sea record for the MIS-6 to 5e deglaciation agree with independent coral and speleothem data[15]. Furthermore, we note that the coral-based sea-level estimates[4] may be suggestive of a sea-level fluctuation of similar amplitude to our inferred sea-level drop around 122.5 kyr (Fig. 2c). The second MIS-5e highstand inferred from the Red Sea record (∼121.5 kyr) resides within a conspicuous gap in the Barbados data[4], but similar work around the Gulf of Aqaba reports terraces up to +10 m that date to 121–122 kyr (ref. 29).

Despite some apparent agreements, the lack of temporal resolution and stratigraphic continuity clearly limits the use of dated coral series for comprehensive validation of our record's finer structure. In addition, the validity of detailed time-series comparisons (as above) might be questioned, given the dating uncertainties. Finally, it has been suggested that rapid sea-level fluctuations may not be represented by well-developed corals[30]. Detailed stratigraphic descriptions of reef/coastal architecture sequences may help, as they yield better insight into the temporal sequence of events.

Such work along the Egyptian coast of the northern Red Sea reveals two main highstand peaks (around +5 to +9 m), separated by a brief 7–10 m sea-level drop[5–7] (see Supplementary Information, Fig. S1). The absolute altitude of the deposits might be affected by uplift, but due to its gradual/long-term nature, uplift cannot account for the centennial-scale relative sequence of two peaks separated by a sharp drop, or for the amplitude of the fluctuations. Note that Red Sea sea-level records based on fossil reefs and coastal deposits[5–7,10–12] are conceptually, technically and tectonically independent from our reconstructions. The reef/coastal sequences[5–7] thus offer strong independent support to the main intra-MIS-5e sea-level fluctuation suggested by our record, with two main highstands (123 and 121.5 kyr) separated by a sharp drop (122.5 kyr) (Fig. 2c). Even the inferred amplitudes of change agree.

Reef-architecture studies on the Eritrean coast of the southern Red Sea[11,12] seem to corroborate not only the two main highstands in our record, but even the minor third peak[11] (Fig. 2c). Although only qualitatively described, the work identifies an initial rapid sea-level rise (their subunit $5e_1$), a drop, a second sea-level rise ($5e_2$), another minor drop, and finally a minor peak with patch reef development ($5e_3$) before the final drop at the end of MIS-5e[11] (see Supplementary Information, Fig. S2). The various reef/coastal sequence studies describe the intra-MIS-5e sea-level drop(s) as erosive/consolidation phases without apparent new reef formation[5–7,11]. Such transient events would probably be missed in time series of dated corals.

Both the structure and amplitude of our KL11 record of MIS-5e sea level (Fig. 2c) are therefore empirically validated (within error margins) by four main observations. These are: the general consensus that sea level reached a longer-term mean position up to +6 m; the observations of individual (peak) deposits up to about +9 m; the suggestions of intra-MIS-5e sea-level variability in a variety of records; and the agreement between our reconstruction and detailed reef/coastal architecture studies regarding the sequence of events within MIS-5e. Moreover, our reconstruction is robust with respect to sedimentation rate within KL11, isostatic effects and regional fluctuations in temperature and net evaporation (see the Supplementary Information).

We now use our record to estimate the rates of MIS-5e sea-level rise. The first time derivative of the short-term smoothed KL11 record shows peak rates of rise of 2.5, 2.0 and 1.1 m per century (Fig. 2c). Mean coral values suggest comparable rates of rise of 1.7 and 1.0 m per century through the intervals 124.7–123.3 and 120.5–119.8 kyr, respectively (Fig. 2). Because overall chronology is critical to the derived rates of sea-level rise, we derive a representative maximum duration for the MIS-5e highstand above 0 m from the literature (see Supplementary Information, Table S1). On the basis of an age range of about 119–128 kyr, this maximum duration is about twice that indicated in Fig. 2. This conservative way of assessing uncertainty in the rates of sea-level rise yields the very minimum estimates for the rates of MIS-5e sea-level rise, being 1.3, 1.0 and 0.6 m per century. We thus infer a full potential range for the rates of rise between 2.5 and 0.6 m per century. We also note that sea-level lowering events reveal a remarkably consistent rate between −1.3 and −1.8 (−0.7 to −0.9) m per century (values in brackets refer to a doubled MIS-5e duration).

Although the intra-MIS-5e oscillations in KL11 seem to be corroborated by coral and reef architecture data, we consider them as only strongly suggestive, because they are not fully replicated in KL09 (see the Methods section). However, two events are common to both records and consequently seem particularly robust (Fig. 2c,d). These are the rise above 0 m at the onset of MIS-5e around 123.5 kyr and the drop ending the main highstand around 119 kyr. The rate of rise above 0 m around 123.5 kyr is 1.5–2.5 (0.8–1.3) m per century, whereas the rate of lowering around 119 kyr is −1.3 to −1.6 (−0.7 to −0.8) m per century. On the basis of only these robust events, therefore, the rate of rise above 0 m from the Red Sea data would be 1.6 ± 0.8, similar to the 1.6 ± 1.0 m per century estimate based on all MIS-5e fluctuations in KL11.

A 1.6 m global sea-level rise per century would correspond to disappearance of an ice sheet the size of Greenland in roughly four centuries (modelling suggests 1,000 years or more[20]). During MIS-5e, such rates of sea-level rise occurred when the global mean temperature was 2 °C higher than today, as expected again by AD 2100 (refs 19,20,22). Using MIS-5e to gain insight into the potential rates of sea-level rise due to further ice-volume reduction in a warming world, our data provide an observational context that underscores the plausibility of recent, unconventionally high, projections of 1.0 ± 0.5 m sea-level rise by AD 2100 (ref. 21).

METHODS

We present stable isotope data for the surface-water dwelling planktonic foraminiferal species *Globigerinoides ruber* (white) in two central Red Sea sediment cores: GeoTü-KL11 (18° 44.5′ N, 39° 20.6′ E, 825 m waterdepth) and GeoTü-KL09 (19° 57.6′ N, 38° 08.3′ E, 814 m waterdepth), which we refer to in abbreviated form as KL11 and KL09. Samples for KL11 were prepared in Tübingen and analysed in Kiel, Germany, on a MAT251 mass spectrometer, over the period 1988–1996. For KL09, a low-resolution pilot series of samples was prepared in Tübingen and analysed in Southampton on a Europa Geo2020 mass spectrometer, in 2006. The high-resolution series for KL09 was prepared and analysed in 2006–2007 in Southampton, using the Geo2020. Each analysis

represents a set of at least 10 and usually more than 20 specimens, and external precision (1σ) is 0.06%. Despite the different equipment, lab protocols, operators and sampling and preparation methods in the two separate sediment cores, the records of KL09 and KL11 agree well, especially when allowing for the external precision (Fig. 1a).

Calibration of $\delta^{18}O_{ruber}$ variations in KL11 into sea-level change is described in detail in refs 15,17,18. The scaling used in that method infers a regional mean annual MIS-5e SST that is up to 0.5 °C warmer than the present (±1 °C at the 1σ level), which is within the range suggested by alkenone-based reconstructions for the nearby easternmost Mediterranean[31]. An extensive pilot study of MIS-5e SST in KL09 is discussed in the Supplementary Information. Calibration of KL09 $\delta^{18}O_{ruber}$ to sea level was done using the calibration method developed for KL11 (refs 15,17,18). It may be expected, however, that absolute $\delta^{18}O_{ruber}$ values at different sites may be offset from one another (for example, as a function of latitude within the basin[16,18] or temperature differences between sites). We use the mean long-term sea-level trend in KL09 in comparison with the coral data to compensate for the potential artefact that was introduced when calibrating KL09 data using the KL11-specific calibration between $\delta^{18}O_{ruber}$ and sea level. A reasonable fit is found when shifting inferred KL09 sea-level values down by about 6 m (Fig. 2b, dashed arrow). As the 1σ margin of the sea-level calibration is about 6 m (refs 17,18), this inferred offset remains comfortably within the overlapping 1σ bands around the KL11 and KL09 sea-level reconstructions. In terms of $\delta^{18}O$, the inferred 6 m offset would imply that KL11 $\delta^{18}O_{ruber}$ is systematically about 0.2% heavier than contemporaneous KL09 $\delta^{18}O_{ruber}$, which would be equivalent to less than 1 °C temperature difference between the sites.

We attribute the difference between the shorter-term fluctuations apparent within MIS-5e in KL11 and KL09 (Fig. 2c,d) to different impacts of bioturbation in the two cores. Sediment accumulation rates through MIS-5e are about 1.5 times higher in KL11 than in KL09 (compare depth axes in Figs 1, 2). As KL11 was sampled in 1 cm steps and KL09 in 0.5 cm steps, the resultant temporal resolution might seem better in KL09 than in KL11 (Fig. 2), but the low-pass filtering effect of bioturbation during sediment accumulation would cause considerable smoothing of high-frequency signals in lower accumulation settings (KL09), whereas these may be preserved under higher accumulation conditions (KL11).

Received 1 May 2007; accepted 11 October 2007; published 16 December 2007.

References

1. Otto-Bliesner, B. L. *et al.* Simulating Arctic climate warmth and icefield retreat in the last interglaciation. *Science* **311**, 1751–1753 (2006).
2. McCulloch, M. T. & Esat, T. The coral record of last interglacial sea levels and sea surface temperatures. *Chem. Geol.* **169**, 107–129 (2000).
3. Stirling, C. H., Esat, T. M., Lambeck, K. & McCulloch, M. T. Timing and duration of the Last Interglacial: Evidence for a restricted interval of widespread coral reef growth. *Earth Planet. Sci. Lett.* **160**, 745–762 (1998).
4. Thompson, W. G. & Goldstein, S. L. Open-system coral ages reveal persistent suborbital sea-level cycles. *Science* **308**, 401–404 (2005).
5. Plaziat, J. C. *et al.* Mise en evidence, sur la côte récifale d'Egypte, d'une régression interrompant le plus haut niveau du Dernier Interglaciaire (5e): Un nouvel indice de variations glacio-eustatiques haute fréquence au Pléistocène? *Bull. Soc. Geol. Fr.* **169**, 115–125 (1998).
6. Plaziat, J. C. *et al.* Quaternary changes in the Egyptian shoreline of the northwestern Red Sea and Gulf of Suez. *Quat. Internat.* **29/30**, 11–22 (1995).
7. Orszag-Sperber, F., Plaziat, J. C., Baltzer, F. & Purser, B. H. Gypsum salina-coral reef relationships during the Last Interglacial (Marine Isotopic Stage 5e) on the Egyptian Red Sea coast: A Quaternary analogue for Neogene marginal evaporites? *Sedim. Geol.* **140**, 61–85 (2001).
8. Neumann, A. C. & Hearty, P. J. Rapid sea-level changes at the close of the last interglacial (substage 5e) recorded in Bahamian island geology. *Geology* **24**, 775–778 (1996).
9. Chen, J. H., Curran, H. A., White, R. & Wasserburg, G. J. Precise chronology of the last interglacial period: ^{234}U–^{230}Th data from fossil coral reefs in the Bahamas. *Geol. Soc. Am. Bull.* **103**, 82–97 (1991).
10. El-Asmar, H. M. Quaternary isotope stratigraphy and paleoclimate of coral reef terraces, Gulf of Aqaba, South Sinai, Egypt. *Quat. Sci. Rev.* **16**, 911–924 (1997).
11. Bruggemann, J. H. *et al.* Stratigraphy, palaeoenvironments and model for the deposition of the Abdur Reef Limestone: Context for an important archaeological site from the last interglacial on the Red Sea coast of Eritrea. *Palaeogeogr. Palaeoclimatol. Palaeoecol.* **203**, 179–206 (2004).
12. Walter, R. C. *et al.* Early human occupation of the Red Sea coast of Eritrea during the last interglacial. *Nature* **405**, 65–69 (2000).
13. Stirling, C. H., Esat, T. M., McCulloch, M. T. & Lambeck, K. High-precision U-series dating of corals from Western Australia and implications for the timing and duration of the Last Interglacial. *Earth Planet. Sci. Lett.* **135**, 115–130 (1995).
14. Cuffey, K. M. & Marshall, S. J. Substantial contribution to sea-level rise during the last interglacial from the Greenland ice sheet. *Nature* **404**, 591–594 (2000).
15. Siddall, M., Bard, E., Rohling, E. J. & Hemleben, Ch. Sea-level reversal during Termination II. *Geology* **34**, 817–820 (2006).
16. Arz, H. W. *et al.* Dominant Northern Hemisphere climate control over millennial-scale glacial sea-level variability. *Quat. Sci. Rev.* **26**, 312–321 (2007).
17. Siddall, M. *et al.* Sea-level fluctuations during the last glacial cycle. *Nature* **423**, 853–858 (2003).
18. Siddall, M. *et al.* Understanding the Red Sea response to sea level. *Earth Planet. Sci. Lett.* **225**, 421–434 (2004).
19. Folland, C. K. *et al.* in *Climate Change 2001, The Scientific Basis. Contribution of Working Group I to the Third Assessment Report of the Intergovernmental Panel on Climate Change* (ed. Houghton, J. T. *et al.*) 99–181 (Cambridge Univ. Press, Cambridge and New York, 2001).
20. Gregory, J. M., Huybrechts, P. & Raper, S. C. B. Threatened loss of the Greenland ice sheet. *Nature* **428**, 616 (2004).
21. Rahmstorf, S. A semi-empirical approach to projecting future sea-level rise. *Science* **315**, 368–370 (2007).
22. Church, J. M. *et al.* in *Climate Change 2001, The Scientific Basis. Contribution of Working Group I to the Third Assessment Report of the Intergovernmental Panel on Climate Change* (ed. Houghton, J. T. *et al.*) 639–693 (Cambridge Univ. Press, Cambridge and New York, 2001).
23. Fairbanks, R. G. A 17,000-year glacio-eustatic sea level record: Influence of glacial melting rates on the Younger Dryas event and deep-ocean circulation. *Nature* **342**, 637–642 (1989).
24. Blanchon, P. & Shaw, J. Reef drowning during the last deglaciation: Evidence for catastrophic sea-level rise and ice-sheet collapse. *Geology* **23**, 4–8 (1995).
25. Stanford, J. D. *et al.* Timing of meltwater pulse 1a and climate responses to meltwater injections. *Paleoceanography* **21**, PA4103 (2006).
26. Cazenave, A. How fast are the ice sheets melting? *Science* **314**, 1250–1252 (2006).
27. Hemleben, Ch. *et al.* Three hundred and eighty thousand year-long stable isotope and faunal records from the Red Sea. *Paleoceanography* **11**, 147–156 (1996).
28. Schellmann, G. & Radtke, U. A revised morpho- and chronostratigraphy of the late and middle Pleistocene coral reef terraces on Southern Barbados (West Indies). *Earth Sci. Rev.* **64**, 157–187 (2004).
29. Scholz, A., Mangini, A. & Felis, T. U-series dating of diagenetically altered fossil reef corals. *Earth Planet. Sci. Lett.* **218**, 163–178 (2004).
30. Hearty, P. J., Neumann, A. C. & O'Leary, M. J. Comment on 'Record of MIS5 sea-level highstands based on U/Th dated coral terraces of Haiti' by Dumas *et al.* [Quaternary International 2006 106–118]. *Quat. Internat.* **162/163**, 205–208 (2007).
31. Rohling, E. J. *et al.* African monsoon variability during the previous interglacial maximum. *Earth Planet. Sci. Lett.* **202**, 61–75 (2002).

Acknowledgements

We thank all colleagues who have offered advice that helped shape the arguments in this manuscript, I. Schmeltzer, S. Geiselhart and H. Erlenkeuser for work on core KL11, and G. Trommer and M. Siccha for work on KL09. H. Elderfield provided valuable feedback to the Mg/Ca pilot study, and I. Marshall and C. Hayward helped with scanning electron microscope and electron microprobe analyses. This study was supported by the UK Natural Environment Research Council (NERC, NE/C003152/1), the German Science Foundation (DFG, He 697/17; Ku 2259/3) and EC project STOPFEN (HPRN-CT-2002-00221).
Correspondence and requests for materials should be addressed to E.J.R. or Ch.H.
Supplementary Information accompanies this paper on www.nature.com/naturegeoscience.

There is one file of Supplementary Information to the paper

High rates of sea-level rise during the last interglacial period

Rohling, E.J., Grant, K., Hemleben, Ch., Siddall, M., Hoogakker, B.A.A., Bolshaw, M., and Kucera, M.

In this file, we present:

(1) a summary of data concerning MIS-5e highstands (Table *S*1)
(2) a summary of coastal/reef architecture sequences for MIS-5e (Figures *S*1, *S*2)
(3) details to help evaluate the robustness of our Red Sea sea-level reconstructions for MIS-5e, with respect to:
    a. sedimentation rates in KL11
    b. isostatic effects
    c. sea surface temperature (shown in Figure *S*3)
    d. net evaporation
(4) supplementary references

The file is presented in a standard Adobe pdf format (prepared on Macintosh), and is 0.8 Mb in size

Supplementary Information to

High rates of sea-level rise during the last interglacial period

Rohling, E.J., Grant, K., Hemleben, Ch., Siddall, M., Hoogakker, B.A.A., Bolshaw, M., and Kucera, M.

Summary of MIS-5e highstand details

Table *S*1 summarises details for the MIS5e highstand from the most relevant studies with respect to the findings reported in our study.

Table *S*1. Summary of literature-based estimates concerning the timing of the MIS-5e maximum highstand interval and the possible presence of interruptions of that maximum highstand. The overall apparent age range of the maximum highstand is around 128 until 119 kyr BP, with an average sea-level position around +4 (-2/+2) m. Within that period, a brief erosive event/sea-level drop seems to have occurred around roughly 122 ±1 kyr BP. Reference numbers correspond to those in the main text.

Best estimate maximum highstand interval (ka)	Region	Highstand value (m)	Reef (R) Beach (B) Notch (N)	Intra-Eemian sea-level drop?	Age of Intra-Eemian sea-level drop (ka)	Ref.
highstand 125-120	Egyptian coast, NW Red Sea	+6 to +9	R, B	Y	~122	s1,s2,s3[a]
highstand 125-118	South Sinai, N Red Sea	+3 to +6	R	N		s5[a]
highstand 125 ± 7	Eritrean coast, SW Red Sea	+10 to +19 (regional uplift)	R	Y (2x)	one ~125 and one younger event	s6[a]
highstand 124-119.5 (small second max. at 115-114.5)	Barbados	up to +7	R	Y	Possible lowstand ~122.5	s7
>0m: 128-120 highstand after isostatic correction: ~125-120	Western Australia	about +4	R	N (but hiatus reported[5])		s8,s9
highstand 127-122	Western Australia + global review	above +2	R	N		s10
highstand 129-120	Bahamas	up to +6	R	Y	~125	s11
132-118 *130-117*	Bahamas	+2 to +6	R, N	Y	~125 *~121*	s12 *rescaled (s9)*

[a.] For summary of other Red Sea reef terrace information, see Walter *et al.*[s4]

Coastal/Reef architecture sequences for MIS-5e

Here we present summary diagrams for the key findings of the coastal/reef architecture sequence studies referred to in the main text, in support of the MIS-5e sea-level fluctuations described in our paper from the Red Sea stable oxygen isotope calibration method (see Figures 2c, *S*3).

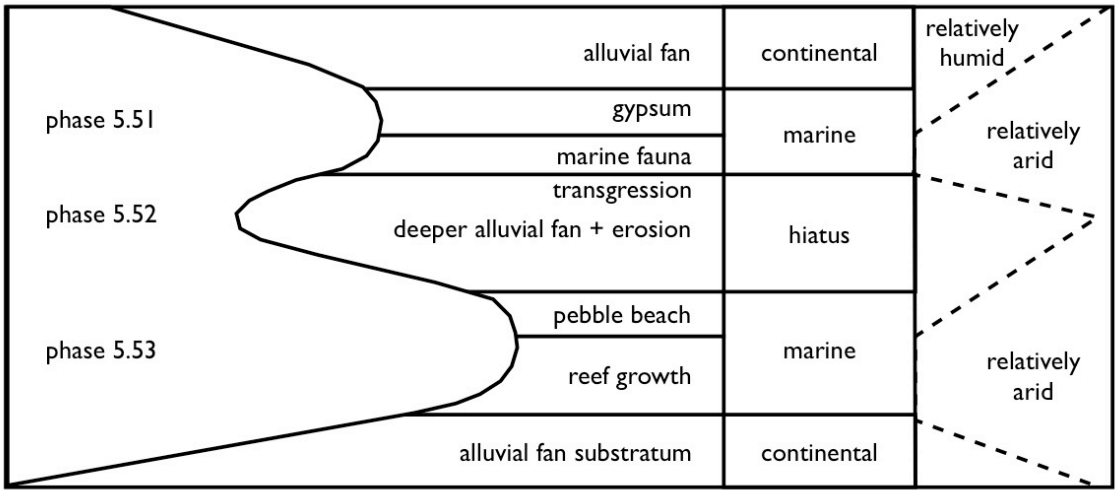

Figure *S1*. Modified after Figure 12 of Orszag-Sperber *et al.*[s3], presenting the summary reconstruction based on coastal/reef architecture studies of MIS-5e along more than 400 km of Egyptian coast of the NW Red Sea[s1-s3]. The work shows a clear distinction of two main highstands (their phases 5.51 and 5.53) separated by a brief sea-level drop (5.52), within MIS-5e. Also shown (right-hand side) is their interpretation of changes in the aridity of the study area, from sedimentological evidence.

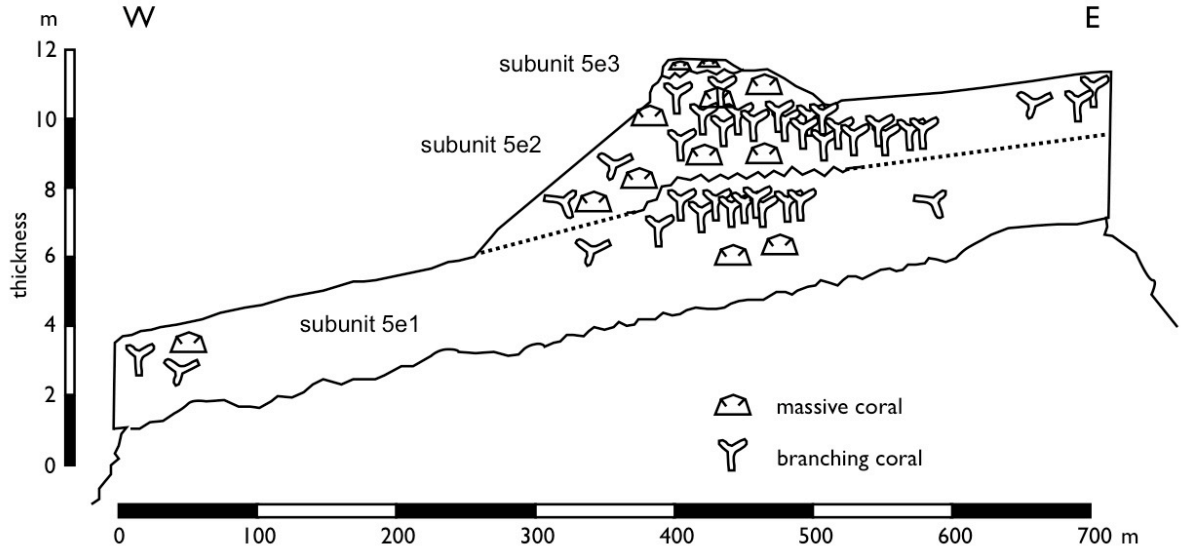

Figure *S2*. Modified after Figure 3 of Bruggemann *et al.*[s6], representing Abdur Reef Limestone transect B in their study region on the Eritrean coast of the SW Red Sea. There is a clear development of a first subunit ($5e_1$) with reef development towards its top, separated by a discontinuity (hardground) from a second reef unit (subunit $5e_2$). Then follows another discontinuity/hardground with a minor phase of patch reef development ($5e_3$). Interestingly, the stratigraphic development through time is supported by a change in the human artefact cultures found within the sequence[s6].

Robustness of the Red Sea sea-level reconstructions

The arguments below complement the empirical support for our record discussed in the main text. This section considers our record's robustness with respect to potential bias from sedimentation rate changes in core KL11, isostatic effects, and from regional fluctuations in sea surface temperature (SST) and net evaporation.

Sedimentation rates in core KL11

In view of the linear calibration between KL11 depth and age (Figures 2a,c; *S*3a,b), it might be construed that a change from low sediment accumulation rates during cold periods to high rates during warm periods might spuriously enhance any rates of changes that are inferred from the record. However, the mean accumulation rate throughout KL11's total 21 m of deposition is 5.6 cm ka^{-1}, and glacials or cold interstadials (cold periods with lower sea level) typically have higher accumulation rates than interglacials (warm periods)[s13]. This may be due to exposure of the large Red Sea shelf areas during periods of lowered sea level, which would cause sediment bypassing of the shelves and consequently enhanced deposition in the deeper basin. However, coarse information is not really good enough. We need to consider whether there have been any detailed changes in the sediment accumulation rate through the MIS-6-5e transition. In agreement with the earlier finding of reduced sediment accumulation rates in KL11 during interglacials[s13], we infer that through MIS-5e about 25 cm of sediment was deposited in about 9,000 years (Figures 2a,c; *S*3a,b), giving a rate of 2.8 cm ka^{-1} (half the mean sedimentation rate of KL11). This value is indistinguishable from that suggested for the immediately preceding MIS 6-5e transition, when about 24 cm appears to have been deposited in about 9,000 years[s14]. It would appear, therefore, that the high rates of sea-level change inferred here cannot be ascribed to any drastic changes in sedimentation rate in KL11.

Isostatic effects.

Our record shows three sea-level rises (123.5, 122, and 120 ka) with roughly similar rates of rise (Figure 2b,c). Isostatic adjustment may have affected the rate of the first event, which forms the continuation of a rapid sea-level rise from the preceding glacial lowstand. However, isostatic effects are too gradual to be the potential cause of the short-term, small-amplitude fluctuations within MIS-5e. This argument is rather similar to that made against uplift impacts on the relative sequence of events in the reef-architecture studies[s1-s3,s6].

SST

Analytical challenges have to date inhibited the development of detailed records for the central Red Sea. Our attempts with organic methods (Uk'37 and Tex86) failed principally due to poor preservation of organic matter. Mg/Ca in foraminiferal shells using conventional techniques (ICP-AES) resulted in highly erratic results. Using scanning electron microscope imaging (backscatter), we found that this is principally due to tiny amounts of high-Mg calcite cement (Mg/Ca ratios > 100 mmol mol^{-1}) in voids or attached to the foraminifera. We then proceeded to measure Mg/Ca in multiple locations of sliced individual specimens of *Globigerinoides ruber* (white, 250-500 μm) using electron microprobe analysis (EMPA, wavelength dispersive), in Cambridge. Foraminifera were ultrasonically cleaned using ultrapure water and mounted in araldite. Samples were polished to expose foraminiferal test walls in cross section and carbon coated. A CAMECA SX100 was used for EMPA using 15 kV accelerating voltage and 10 nA beam current with beamsize of 5μm. Spot measurements of weight % Ca (detection limit 819 ppm) and Mg (detection limit 45 ppm) were carried out spread across the foraminiferal chambers in order to accommodate for heterogeneity[s15,s16].

Individually averaged foraminiferal Mg/Ca ratios were then converted into SST using the calibration of McConnell and Thunell[s17].

The record we present (Figure *S*3c) is based on a comprehensive pilot series of 441 electron microprobe Mg/Ca measurements from 40 thin-sectioned specimens of *G. ruber* (white). It represents the first reasonably coherent Mg/Ca-based SST series for the central Red Sea. The variability of the individual-specimen Mg/Ca data includes much bias due to seasonality, which is suppressed in the $\delta^{18}O$ data where each analysis represents a collection of more than 10 (usually more than 20) specimens. Unless means of at least 20 specimens can be determined per sample (requiring a major specialised analytical project), individual-specimen Mg/Ca data will remain too noisy for high-resolution comparisons with the $\delta^{18}O$ record. However, there is some merit in comparing long-term averaged trends, where the temporal averaging reduces individual-point bias. Such a first-order comparison (Figure *S*3a,c) suggests that the light $\delta^{18}O$ values underlying the long-term sea-level highstand in the Red Sea record cannot be ascribed to an SST-induced artefact. Higher Mg/Ca based SST at the end of the deglaciation might be due to salinity effects[s18]. Evaluation of such potential effects would require a major specialised project of similar EMPA on foraminifera from plankton-tows and core tops in the Red Sea, alongside systematic measurements of a variety of environmental parameters (e.g., salinity, water-column and pore-water (carbonate) chemistry, etc.).

In the current absence of reliable records of mean annual SST in the central Red Sea through extended intervals of time (including MIS-5e), a broader regional view is required. Such a broader perspective suggests that the intra-MIS-5e fluctuations are unlikely to be due to SST variations. The $\delta^{18}O$ shifts underlying the calculated short-term sea-level rises within MIS-5e amount to 0.5‰ (Figures 1c,d; 2a,c; *S*3b). This would be equivalent to mean sea surface warming by 2°C, or nearly 3°C when accounting for increased evaporation during warm periods (below). Such variability seems improbably large given that the full glacial-interglacial mean SST change in the Red Sea was only about 5°C[Refs.s19-s21] , and only 4°C or less in the Arabian Sea[s22,s23]. Indeed, multiple replicated SST reconstructions for the nearby eastern Mediterranean suggest limited mean annual SST variability within MIS-5e of less than ±0.5°C[Ref.s24], which is well within the ±1°C uncertainty allowed in our 1σ sea-level uncertainty (Figures 2a,c; *S*3a,b).

We also note that a northern Red Sea coral-based study reconstructs colder winters and warmer summers during MIS-5e, relative to the present and the Late Holocene, but not much of a change in mean annual SST[Ref.s25]. If anything, comparison between apparent mean coral $\delta^{18}O$ values (their Figure 2)[s25] would suggest that MIS-5e was about 0.5‰ *heavier* (i.e., about 2°C *colder*) than the present. A similar comparison with the Late Holocene (their Figure 2)[s25] suggests that MIS-5e was about 0.2‰ *lighter*, or just under 1°C *warmer*. These apparent mean contrasts between MIS-5e and either the present-day or the Late Holocene do not substantially deviate from the assertions about mean MIS-5e SST made in the present paper (*Methods*).

Finally, we emphasise that *Globigerinoides ruber* lives throughout the year in Red Sea surface waters (also during MIS-5e, as suggested by our observed range of Mg/Ca temperature values of individual specimens; Figure *S*3b). By developing our $\delta^{18}O$ records using sets of commonly 20 or more specimens per analysis (*Methods*), seasonal imprints are effectively averaged out, and thus cannot explain the $\delta^{18}O$ shifts.

Net evaporation

Finally, we consider whether it would be realistic to attribute the observed $\delta^{18}O$ shifts within MIS-5e to changes in net evaporation. This again seems to be rather unlikely. Firstly, conditions would need to change beyond modern seasonal extremes for impacts outside the sea-level confidence limits (here, the "beyond seasonal extremes" stands for hypothetical states in which the basis was assumed to be "locked" for the entire year in either the modern extreme winter conditions, or the modern extreme summer conditions)[s26,s27]. Even the inferred increase in MIS-5e seasonal contrast in the Red Sea[s25] would not get anywhere close to these extreme hypothetical states. Secondly, detailed stratigraphic investigation of fossil Red Sea reefs and associated salinas suggests that the MIS-5e highstands coincided with relatively arid episodes[s3] (see Figure *S*1) This association may be understood in terms of ageostrophic (cross-basin) surface airflows, which are strongly divergent over the Red Sea basin due to much enhanced heating of the land relative to the sea, and which result in enhanced evaporation[s28]. During the warmest phases of the MIS-5e insolation maximum, such effects would maximise evaporation.

Overall, the assessment above combines with the empirical support from coral data and reef architecture studies (main text and Figures *S*1, *S*2) to present a strong case in support of our inferred sequence of intra-MIS-5e sea-level fluctuations (Figures 2c, *S*3b).

Supplementary References

s1. Plaziat, J. C. *et al.* Mise en evidence, sur la côte récifale d'Egypte, d'une régression interrompant le plus haut niveau du Dernier Interglaciaire (5e): un nouvel indice de variations glacio-eustatiques haute fréquence au Pléistocène? *Bull. Soc. Géol. Fr.* **169**, 115-125 (1998).

s2. Plaziat, J. C. *et al.* Quaternary changes in the Egyptian shoreline of the northwestern Red Sea and Gulf of Suez, *Quat. Internat.* **29/30**, 11-22 (1995).

s3. Orszag-Sperber, F., Plaziat, J. C., Baltzer, F. & Purser, B. H. Gypsum salina-coral reef relationships during the Last Interglacial (Marine Isotopic Stage 5e) on the Egyptian Red Sea coast: a Quaternary analogue for Neogene marginal evaporites? *Sed. Geol.* **140,** 61-85 (2001).

s4. Walter, R. C. *et al.* Early human occupation of the Red Sea coast of Eritrea during the last interglacial. *Nature* **405**, 65-69 (2000).

s5. El-Asmar, H. M., Quaternary isotope stratigraphy and paleoclimate of coral reef terraces, Gulf of Aqaba, South Sinai, Egypt. *Quat. Sci. Rev.* **16**, 911-924 (1997).

s6. Bruggemann, J. H. *et al.* Stratigraphy, palaeoenvironments and model for the deposition of the Abdur Reef Limestone: context for an important archaeological site from the last interglacial on the Red Sea coast of Eritrea. *Palaeogeogr. Palaeoclimatol. Palaeoecol.* **203**, 179-206 (2004).

s7. Thompson, W. G. & Goldstein, S. L. Open-system coral ages reveal persistent suborbital sea-level cycles. *Science* **308**, 401-404 (2005).

s8. McCulloch, M. T. & Esat, T. The coral record of last interglacial sea levels and sea surface temperatures. *Chem. Geol.* **169**, 107-129 (2000).

s9. Stirling, C. H., Esat, T. M., Lambeck, K. & McCulloch, M. T. Timing and duration of the Last Interglacial: evidence for a restricted interval of widespread coral reef growth. *Earth Planet. Sci. Lett.* **160**, 745-762 (1998).

s10. Stirling, C. H., Esat, T. M., McCulloch, M. T. & Lambeck, K. High-precision U-series dating of corals from Western Australia and implications for the timing and duration of the Last Interglacial. *Earth Planet. Sci. Lett.* **135**, 115-130 (1995).
s11. Neumann, A. C. & Hearty, P. J. Rapid sea-level changes at the close of the last interglacial (substage 5e) recorded in Bahamian island geology. *Geology* **24**, 775-778 (1996).
s12. Chen, J. H., Curran, H. A., White, R. & Wasserburg, G. J. Precise chronology of the last interglacial period: ^{234}U-^{230}Th data from fossil coral reefs in the Bahamas. *Geol. Soc. Am. Bull.* **103**, 82-97 (1991).
s13. Hemleben, Ch. *et al.* Three hundred and eighty thousand year-long stable isotope and faunal records from the Red Sea. *Paleoceanography* **11**, 147-156 (1996).
s14. Siddall, M., Bard, E., Rohling, E. J. and Hemleben, Ch., Sea-level reversal during Termination II, *Geology* **34**, 817-820 (2006).
s15. Brown, S. J., Elderfield, H. Variations in Mg/Ca and Sr/Ca ratios of planktonic foraminifera caused by postdepositional dissolution: evidence of shallow Mg-dependent dissolution. *Paleoceanography **11***, 543-551 (1996).
s16. Anand, P., Elderfield, H. Variability of Mg/Ca and Sr/Ca between and within the planktonic foraminifers Globigerina bulloides and Globorotalia truncatulinoides. *G*^{3} **6**, doi:10.1029/2004GC000811 (2005).
s17. McConnell, M. C. and Thunell, R. C. Calibration of the planktonic foraminiferal Mg/Ca paleothermometer: sediment trap results from the Guaymas Basin, Gulf of California. *Paleoceanography* **20**, PA2016, doi:10.1029/2004PA001077 (2005).
s18. Lea, D. W., Mashiotta, T. A., Spero, H. J. Controls on magnesium and strontium uptake in planktonic foraminifera determined by live culturing. *Geochimica et Cosmochimica Acta* **63**, 2369-2379 (1999).
s19. Arz, H. W. *et al.* Dominant Northern Hemisphere climate control over millennial-scale glacial sea-level variability. *Quat. Sci. Rev.* **26**, 312-321 (2007).
s20. Arz, H. W. *et al.* Mediterranean moisture source for an early-Holocene humid period in the northern Red Sea. *Science* **300**, 118-121 (2003).
s21. Arz, H. W. *et al.* Influence of Northern Hemisphere climate and global sea level rise on the restricted Red Sea marine environment during termination I. *Paleoceanography* **18**, 1053, doi:10.1029/2002PA000864 (2003).
s22. Cayre, O. and Bard, E. Planktonic foraminiferal and alkenone records of the last deglaciation from the eastern Arabian Sea. *Quat. Res.* **52**, 337-342 (1999).
s23. Schulte, S. and Mueller P. J. Variations of sea surface temperature and primary productivity during Heinrich and Dansgaard-Oeschger events in the northeastern Arabian Sea. *Geo-Marine Lett.* **21**, 168-175 (2001).
s24. Rohling, E. J. *et al.* African monsoon variability during the previous interglacial maximum. *Earth Planet. Sci. Lett.* **202,** 61-75 (2002).
s25. Felis, T. *et al.* Increased seasonality in Middle East temperatures during the last interglacial period. *Nature* **429**, 164-168 (2004).
s26. Siddall, M. *et al.* Sea-level fluctuations during the last glacial cycle. *Nature* **423**, 853-858 (2003).
s27. Siddall M. *et al.* Understanding the Red Sea response to sea level. *Earth Planet. Sci. Lett.* **225,** 421-434 (2004).
s28. Eshel, G. and Heavens, N. Climatological evaporation seasonality in the northern Red Sea. *Paleoceanography* in press (2007).

Supplementary Figure *S*3
(a) and **(b)** as main-text Figures 2a,c.
(c) Sea surface temperatures determined from our pilot study of multiple electron microprobe Mg/Ca analyses on 40 individual specimens of *G. ruber* (white). Symbols indicate the mean value per sample, based on between 6 and 20 measurements per specimen, and between 1 and 4 specimens per sample. Error bars indicate standard error of the mean. The heavy blue line represents a 3000-year moving Gaussian filter through the data, for comparison with the long-term sea-level change indicated in **(a)**.